Kirchhoff prestack depth migration in 3-D simple models: comparison of triclinic anisotropy with simpler anisotropies

Václav Bucha

Department of Geophysics, Faculty of Mathematics and Physics, Charles University, Ke Karlovu 3, 121 16 Praha 2, Czech Republic (http://sw3d.cz/staff/bucha.htm)

Received: September 2, 2011; Revised: January 4, 2012; Accepted: February 1, 2012

ABSTRACT

We use Kirchhoff prestack depth migration to calculate migrated sections in 3-D simple anisotropic homogeneous velocity models in order to demonstrate the impact of anisotropy on migrated images. The recorded wave field is generated in models composed of two homogeneous layers separated by one either non-inclined or inclined curved interface. The anisotropy in the upper layer is triclinic. We apply Kirchhoff prestack depth migration to velocity models with different types of anisotropy: a triclinic anisotropic medium, an isotropic medium, transversely isotropic media with a horizontal (HTI) and vertical (VTI) symmetry axis. We observe asymmetry in migration caused by triclinic anisotropy and we show the errors of the migrated interface caused by inaccurate velocity models used for migration. The study is limited to P-waves.

Keywords: 3-D Kirchhoff prestack depth migration, anisotropic velocity model

1. INTRODUCTION

Inaccurate velocity models used for migration can lead to position errors of interfaces in migrated sections. Anisotropy-induced distortions in imaging have been analyzed mostly for 2-D transverse isotropic (TI) media (e.g., *Larner and Cohen, 1993*; *Alkhalifah and Larner, 1994*) and for transverse isotropic media with a tilted symmetry axis (TTI) (e.g., *Ball, 1995*; *Isaac and Lawton, 1999*; *Vestrum et al., 1999*; *Behera and Tsvankin, 2009*; *Vestrum and Lawton, 2010*).

Tsvankin et al. (2010) mention that TI models with a vertical (VTI) and tilted (TTI) axis of symmetry have become practically standard in prestack imaging projects all over the world. On the other hand, *Tsvankin et al. (2010)* also write that many sedimentary formations including sands and carbonates contain vertical or steeply dipping fracture sets and should be described by effective symmetries lower

than TI, such as orthorhombic. In this paper we show the potential consequences of migrating 3-D data using TI velocity models while the actual medium is of a lower anisotropy symmetry.

We generate 3-D synthetic data using an approximate ray theory. To calculate the synthetic recorded wave field, we use a 3-D simple anisotropic velocity model composed of two homogeneous layers separated by one curved interface that is either non-inclined or inclined. The anisotropy in the upper layer is triclinic (the lowest symmetry) and is relatively strong. The bottom layer is isotropic.

We migrate the synthetic data using 3-D ray-based Kirchhoff prestack depth migration. To evaluate anisotropy-induced distortions of the imaged curved interface, we use several anisotropic migration velocity models. They all consist of a single homogeneous layer but of different anisotropy symmetry: triclinic (identical to the actual velocity above the interface), isotropic, and transversely isotropic with horizontal (HTI) and vertical (VTI) symmetry axis.

The asymmetry caused by triclinic anisotropy, that is mirror asymmetric with respect to vertical planes, is observed for the individual migrated sections (subsequently stacked to obtain the 3-D migration section). We show mispositioning, distortion and defocusing of the migrated interface caused by inaccurate velocity models used for migration. We use 3-D migration because the reflected two-point rays propagate in triclinic media in a 3-D volume. The study is limited to P-waves.

The first tests of this migration algorithm on 2-D and 3-D models of various anisotropy were reported by *Bucha (2010)*.

The GOCAD program has been used to visualize the 3-D model with curved interface, shot-receiver configurations, computed two-point rays and the migration data cube (GOCAD voxet).

2. ANISOTROPIC VELOCITY MODELS

The dimensions of the 3-D velocity models and measurement configurations are derived from the 2-D Marmousi model and dataset (*Versteeg and Grau, 1991*). The horizontal dimensions of the model are 9.2 km × 10 km and the depth is 3 km. The velocity model is composed of two homogeneous layers separated by one curved interface. We use two models, one with a non-inclined curved interface and one with an inclined curved interface (see Fig. 1).

The recorded wave field is computed in the model with the triclinic anisotropy in the upper layer:

a) Triclinic anisotropy (TA) representing dry Vosges sandstone (*Mensch and Rasolofosaon, 1997*). The matrix of density-reduced elastic moduli in km^2/s^2 reads

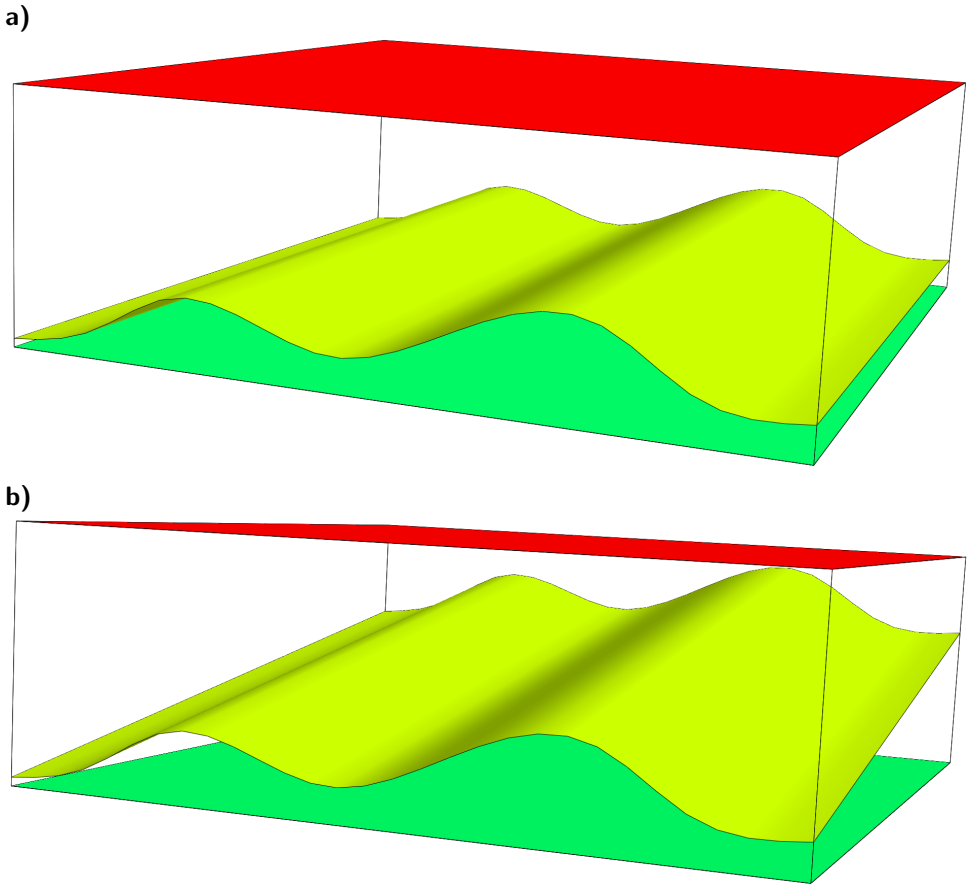

Fig. 1. 3-D models with **a)** a non-inclined curved interface, and with **b)** an inclined curved interface. The horizontal dimensions of the models are 9.2 km × 10 km, the depth is 3 km. The models consist of three interfaces: one curved interface, and the top and bottom model planes. The interfaces are coloured according to the GOCAD surface indices.

$$\begin{pmatrix} 10.3 & 0.9 & 1.3 & 1.4 & 1.1 & 0.8 \\ & 10.6 & 2.1 & 0.2 & -0.2 & -0.6 \\ & & 14.1 & 0.0 & -0.5 & -1.0 \\ & & & 5.1 & 0.0 & 0.2 \\ & & & & 6.0 & 0.0 \\ & & & & & 4.9 \end{pmatrix}.$$

The bottom layer is isotropic and has P-wave velocity $V_p = 3.6$ km/s.

The migration is performed using single-layer homogeneous models (without an interface). The reference migration velocity consists of the triclinic (TA) layer in item a) above. In addition, the following single-layer models are used:

b) Isotropic medium (ISO) with P-wave velocity ${V_p}^2 = 14.1$ km^2/s^2 (equal to the vertical P-wave velocity in the TA model, matrix element A_{33}), and S-wave velocity ${V_s}^2 = 5.55$ km^2/s^2 (mean of matrix elements A_{44} and A_{55} in the TA model).

c) VTI-1 is a transversely isotropic medium with a vertical symmetry axis (VTI). The matrix of elastic moduli reads

$$\begin{pmatrix} 10.45 & 0.65 & 1.7 & 0.0 & 0.0 & 0.0 \\ & 10.45 & 1.7 & 0.0 & 0.0 & 0.0 \\ & & 14.1 & 0.0 & 0.0 & 0.0 \\ & & & 5.55 & 0.0 & 0.0 \\ & & & & 5.55 & 0.0 \\ & & & & & 4.9 \end{pmatrix}.$$

We fitted matrix element A_{33} for vertical P-waves and elements $A_{13} = A_{23}$ (mean of triclinic elements A_{13}, A_{23}) for near vertical P-waves according to the elastic moduli of triclinic anisotropy. Horizontal P-wave velocities (elements A_{11}, A_{22}) are equal in both directions and the value is the mean of triclinic elements A_{11}, A_{22}.

d) VTI-2 is similar to VTI-1, we only decreased matrix element A_{33}, which is responsible for the vertical P-wave velocity, to $A_{33} = 11.6$ km^2/s^2.

e) VTI-3 is similar to VTI-1, we only decreased matrix elements A_{11} and A_{12}, which are responsible for the horizontal P-wave velocity in the direction parallel with the measurement lines, to $A_{11} = 8.95$ km^2/s^2 and $A_{12} = -0.85$ km^2/s^2.

f) HTI-1 is a transversely isotropic medium with a horizontal symmetry axis (HTI). The symmetry axis is parallel with the x_1 coordinate axis. The matrix of the elastic moduli reads

$$\begin{pmatrix} 10.3 & 1.3 & 1.3 & 0.0 & 0.0 & 0.0 \\ & 14.1 & 3.9 & 0.0 & 0.0 & 0.0 \\ & & 14.1 & 0.0 & 0.0 & 0.0 \\ & & & 5.1 & 0.0 & 0.0 \\ & & & & 6.0 & 0.0 \\ & & & & & 6.0 \end{pmatrix}.$$

We fitted matrix element A_{33} for vertical P-waves and element A_{23} for near vertical P-waves according to the elastic moduli of triclinic anisotropy. The horizontal P-wave velocity, perpendicular to the profile lines (element A_{22}), is equal to the vertical P-wave velocity (element A_{33}) of the triclinic (TA) model.

g) HTI-2 is a transversely isotropic medium with a horizontal symmetry axis (HTI). The symmetry axis is parallel with the x_2 coordinate axis. The matrix of the elastic moduli reads

$$\begin{pmatrix} 14.1 & 2.1 & 2.1 & 0.0 & 0.0 & 0.0 \\ & 10.6 & 2.1 & 0.0 & 0.0 & 0.0 \\ & & 14.1 & 0.0 & 0.0 & 0.0 \\ & & & 5.1 & 0.0 & 0.0 \\ & & & & 6.0 & 0.0 \\ & & & & & 5.1 \end{pmatrix}.$$

We fitted matrix element A_{33} for vertical P-waves and element A_{13} for near vertical P-waves according to the elastic moduli of triclinic anisotropy. The horizontal P-wave velocity, parallel with the profile lines (element A_{11}), is equal to the vertical P-wave velocity (element A_{33}) of the triclinic (TA) model.

In models ISO, VTI-1, HTI-1 and HTI-2 we chose the density-reduced elastic moduli (for vertical and near vertical P-waves) which yield approximately correct depths of the interface in the migrated image. Model VTI-2 with the lower velocity for vertical P-waves is proposed to show undermigration. Model VTI-3 demonstrates the influence of the lower velocity for horizontal P-waves.

3. SHOTS AND RECEIVERS

The measurement configuration is derived from the Marmousi model and dataset (*Versteeg and Grau, 1991*). The profile lines are parallel with the x_1 coordinate axis. Each profile line has the following configuration: The first shot is 3 km from the left-hand side of the velocity model, the last shot is 8.975 km from the left-hand side of the velocity model, the distance between the shots is 0.025 km, and the depth of the shots is 0 km. The total number of shots along one profile line is 240. The number of receivers per shot is 96, the first receiver is located 2.575 km left of the shot location, the last receiver is 0.2 km left of the shot location, the distance between the receivers is 0.025 km, and the depth of the receivers is 0 km. This configuration simulates a simplified towed streamed acquisition geometry.

The 3-D measurement configuration consists of 81 parallel profile lines, see Figs. 2 and 3. The distance between the parallel profile lines is 0.025 km.

4. RECORDED WAVE FIELD

The recorded wave field in the triclinic velocity model was computed using the ANRAY software package (*Gajewski and Pšenčík, 1990*). 3-D ray tracing is used to calculate the two-point rays of the reflected P-wave. We then compute the ray-theory seismograms at the receivers. The two-point rays do not stay in the vertical planes corresponding to the individual profiles (see Fig. 4).

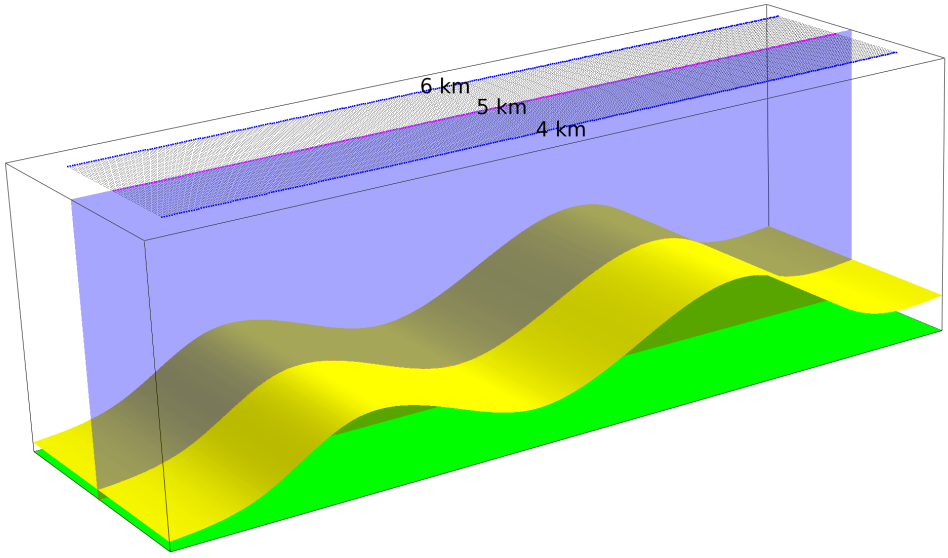

Fig. 2. A slice of the 3-D model with 81 parallel profile lines, the non-inclined curved interface and the bottom model plane. The horizontal dimensions of the model slice are 9.2 km × 3 km, the depth is 3 km. We compute and stack the migrated sections in the 2-D plane located in the middle of the shot-receiver configuration (at horizontal coordinate $x_2 = 5$ km).

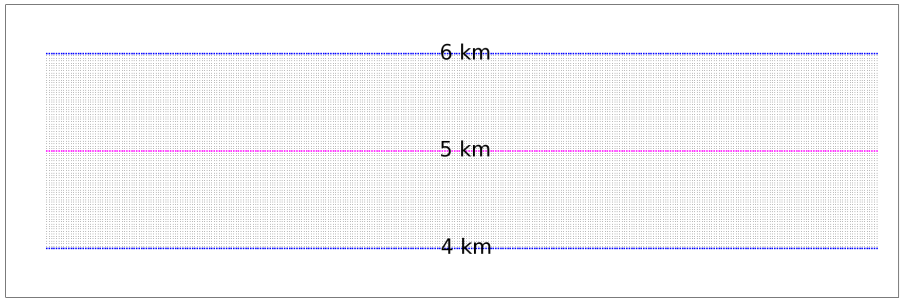

Fig. 3. Top view of the 81 parallel profile lines parametrized by the x_2 coordinate.

In the velocity model with the non-inclined curved interface, the recorded wave field is equal for all parallel profile lines, since the layers are homogeneous and the non-inclined curved interface is independent of the distance x_2 perpendicular to the profile lines (2.5-D model, see Figs. 1a, 2).

In the model with inclined curved interface, the recorded wave field must be calculated for each profile line independently (see Fig. 1b).

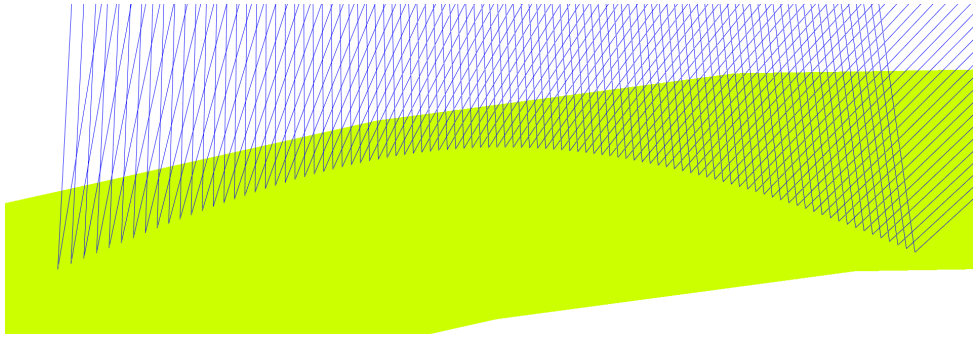

Fig. 4. Detailed view of two-point rays computed in the model with triclinic anisotropy. Note the curved path of reflections at the interface.

5. 3-D KIRCHHOFF PRESTACK DEPTH MIGRATION

We use the MODEL, CRT, FORMS and DATA packages for the Kirchhoff prestack depth migration (*Červený et al., 1988*; *Bulant, 1996*). The migration consists of two-parametric ray tracing from the individual surface points, calculating grid values of travel times and amplitudes, performing common-shot migration and stacking of migrated images. The shot-receiver configuration consists of 81 parallel profile lines at intervals of 0.025 km (see Figs. 2, 3). The first profile line starts at horizontal coordinate $x_2 = 4$ km and the last profile line ends at horizontal coordinate $x_2 = 6$ km.

For the purpose of our analysis, we calculate only one vertical image section corresponding to the central profile line ($x_2 = 5$ km, see Fig. 2). Although only a 2-D line, such an image represents one vertical section of full 3-D migrated volume. We form the image by computing and summing the corresponding contributions (images) from all 81 parallel source-receiver lines. While summing the contributions, the constructive interference focuses the migrated interface and the destructive interference reduces undesirable migration artifacts (non-specular reflections). We also use cosine taper to clear some residua.

5.1. Migration Using Correct Velocity Model with Triclinic Anisotropy

We first choose the anisotropy in the homogeneous velocity model for the migration equal to the triclinic anisotropy in the upper layer of the velocity model used to compute the recorded wave field. Fig. 5 shows stacked migrated sections calculated in the models with non-inclined and inclined curved interfaces. 81×240 common-shot prestack depth migrated sections, corresponding to 81 profile lines and 240 sources along each profile line, have been stacked. The migrated interface coincides nearly perfectly with the interface in the model used to compute the recorded wave field. The migrated sections in Fig. 5 demonstrate that the migration algorithm

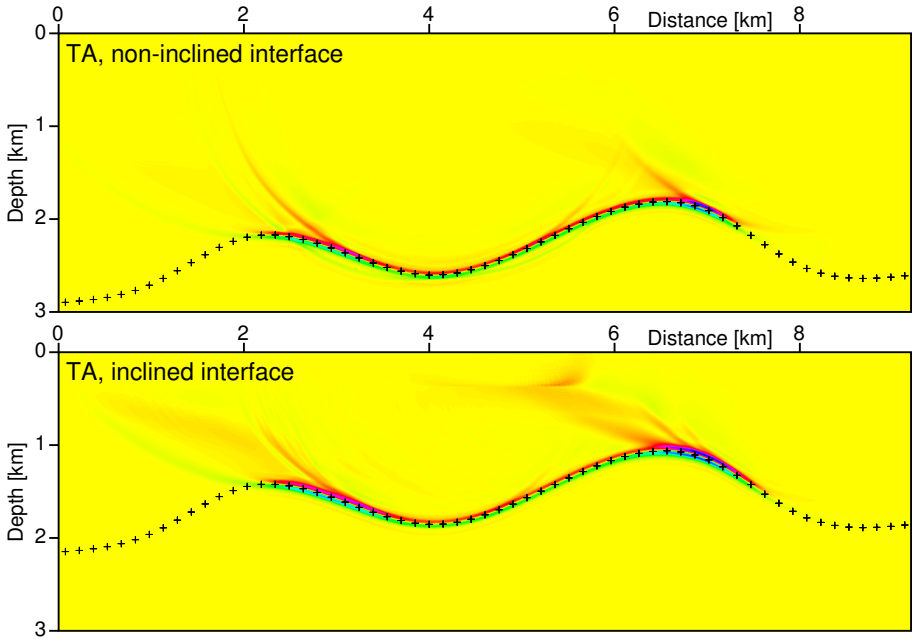

Fig. 5. Stacked migrated sections calculated in the models with non-inclined and inclined curved interface. 81×240 common-shot prestack depth migrated sections, corresponding to 81 profile lines and 240 sources along each profile line, have been stacked. The triclinic anisotropy in the upper layer of the velocity model used to compute the recorded wave field is the same as the anisotropy in the homogeneous velocity model used for migration. The crosses denote the interface in the velocity model used to compute the recorded wave field.

works well. These migrated sections may be used as a reference for comparison with the migrated sections calculated for inaccurate velocity models.

To demonstrate the impact of triclinic anisotropy (TA) on imaging, we compare the individual contributions to the image at $x_2 = 5$ km from eight source-receiver lines (240 shots per each line) symmetrically distributed around the image line (Figs. 6 and 7). The images are computed for the model with non-inclined curved interface.

Despite the symmetrical distribution of the source-receiver lines around the image line $x_2 = 5$ km, Figs. 6 and 7 show apparent differences in the contributions from the corresponding symmetric pairs (compare the contributions from lines 4.6 and 5.4, lines 4.4 and 5.6, etc.).

In comparison with Fig. 6, the migrated interfaces in Fig. 7 are shifted, distorted and poorly displayed in the horizontal range of approximately 4–6 km. These migration distortions are larger with greater distance from the middle profile line. The crosses denote the interface in the velocity model used for computation of the recorded wave field.

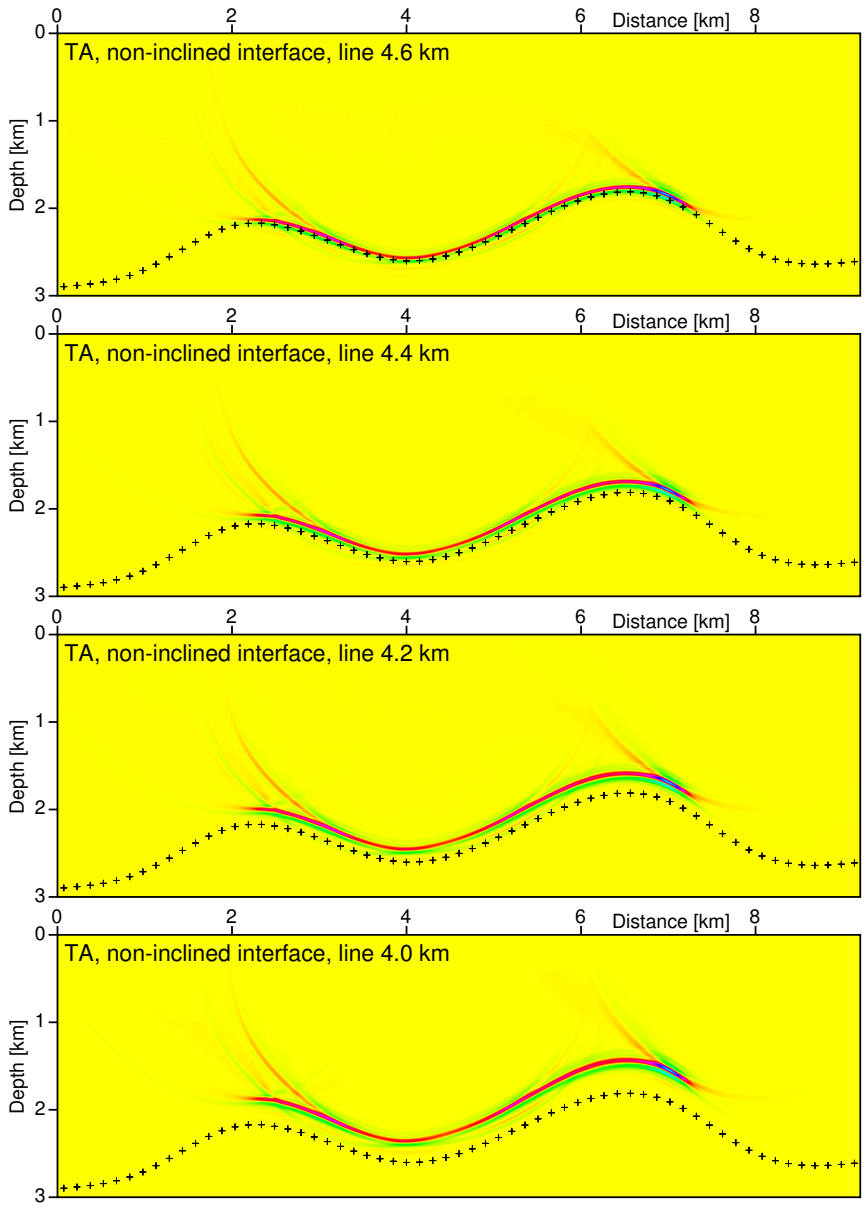

Fig. 6. Individual images corresponding to the source-receiver lines at $x_2 = 4.6$, 4.4, 4.2 and 4.0 km (each image is a stack of 240 images from 240 shots located along each line). The images are shown at the vertical plane $x_2 = 5$ km and represent four individual contributions (out of 81) to the final image at $x_2 = 5$ km. The triclinic anisotropy in the upper layer of the velocity model used to compute the recorded wave field is the same as the anisotropy in the velocity model used for migration. The crosses denote the interface in the velocity model used to compute the recorded wave field. The curved interface is non-inclined.

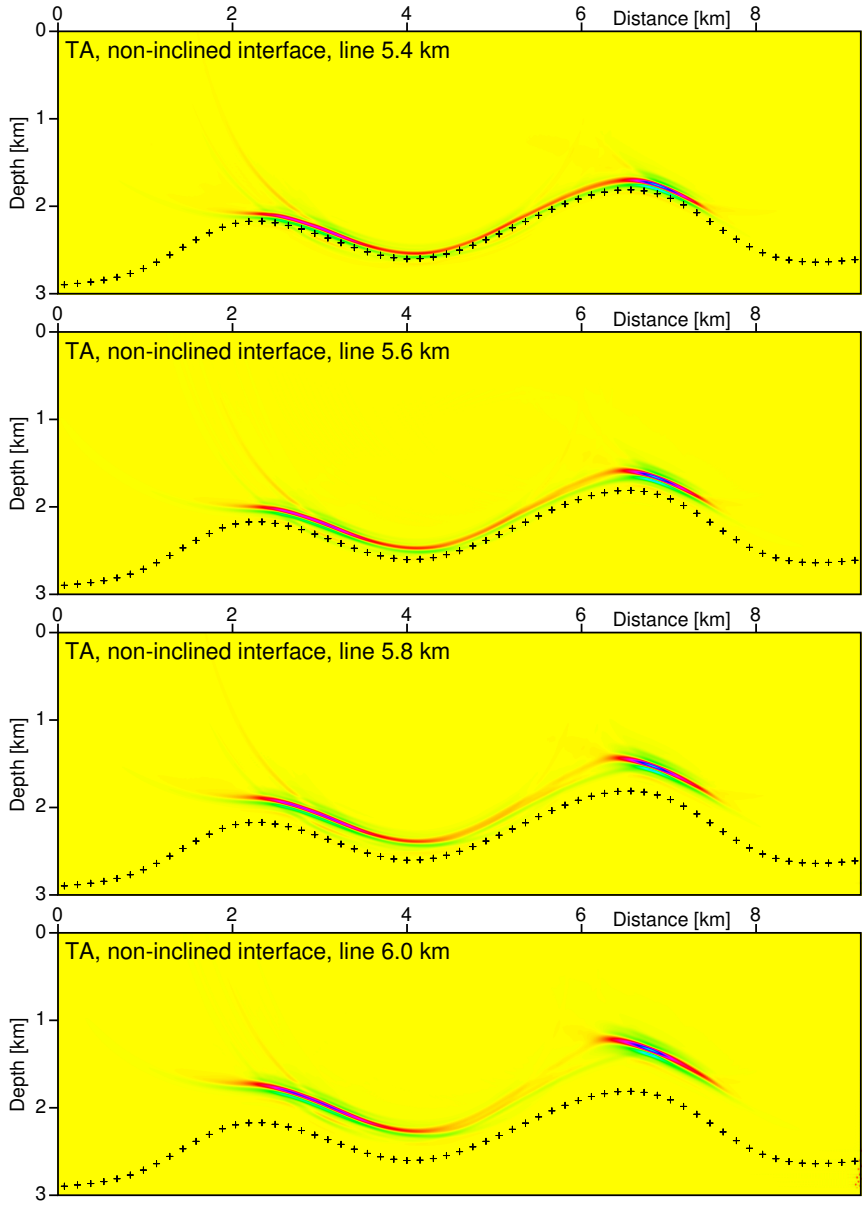

Fig. 7. Individual images corresponding to the source-receiver lines at $x_2 = 5.4$, 5.6, 5.8 and 6.0 km (each image is a stack of 240 images from 240 shots located along each line). The images are shown at the vertical plane $x_2 = 5$ km and represent four individual contributions (out of 81) to the final image at $x_2 = 5$ km. The triclinic anisotropy in the upper layer of the velocity model used to compute the recorded wave field is the same as the anisotropy in the velocity model used for migration. The crosses denote the interface in the velocity model used to compute the recorded wave field. The curved interface is non-inclined.

Another effect of the triclinic asymmetry is the shift of the reflection points away from the vertical plane containing the source-receiver line even for non-inclined interfaces, i.e. incident and reflected rays do not lie in a vertical plane. Specifically for our model of triclinic anisotropy, specular reflections from the non-inclined interface occurring at $x_2 = 5$ km in the subsurface are actually recorded by receivers on the surface located close to $x_2 = 4.9$ km. Of course, for all other models (VTI-1,2,3 and HTI-1,2) where the anisotropy is symmetric with respect to x_2, the specular reflections will be recorded by receivers located along lines right above the reflection points, i.e. the incident and reflected rays lie in a vertical plane. This effect of the triclinic anisotropy is thus similar to the effect of an inclined interface in an isotropic medium.

Fig. 8 shows sections and cross-sections of the 3-D migrated volume for the non-inclined curved interface corresponding to the profile line at $x_2 = 5$ km. The common-shot prestack depth migrated volumes corresponding to 240 sources along the profile line have been stacked. Notice a slight shift of the stationary point to the left of $x_2 = 5$ km on all cross-sections (Fig. 8a).

5.2. Migration Using Incorrect Velocity Anisotropy

Figs. 9,11,13,14 show stacked migrated sections when the anisotropy in the homogeneous velocity model used for migration is different from the anisotropy in the upper layer of the velocity model used to compute the recorded wave field. Specifically, we compare the results of the migration using the correct triclinic (TA) model with those using incorrect isotropic (ISO) and transversely isotropic models with vertical and horizontal symmetry axes (VTI-1,2,3 and HTI-1,2) previously introduced in Section 2. These experiments are to simulate situations in which we have made an incorrect guess of the anisotropic velocity model for migration. We shall divide the results of our tests according to the values of the vertical and horizontal P-wave velocities.

5.2.1. Incorrect Assumption of VTI Symmetry or HTI Symmetry with the Axis Parallel with the Profile Lines

In this study, the vertical P-wave velocity (matrix element A_{33}) in the VTI-1 and HTI-1 models is the same as the analogous velocity (A_{33}) in the triclinic (TA) model. The horizontal P-wave velocity parallel with the profile lines (matrix element A_{11}) in the VTI-1 model is nearly the same, and in the HTI-1 model it is the same, as the horizontal P-wave velocity (A_{11}) in the triclinic (TA) model.

In models VTI-1 and HTI-1 we chose such density-reduced elastic moduli that result in approximately correct depths of the interface in the migrated images. The migrated sections are very similar whether we migrate in the model with the VTI-1 or HTI-1 anisotropy (see Fig. 9). Note the poorly displayed migrated interface in the horizontal range of approximately 4−6 km. The discussed segment of the interface (4−6 km) is worse for the model with the inclined curved interface. The migrated interface is slightly mispositioned.

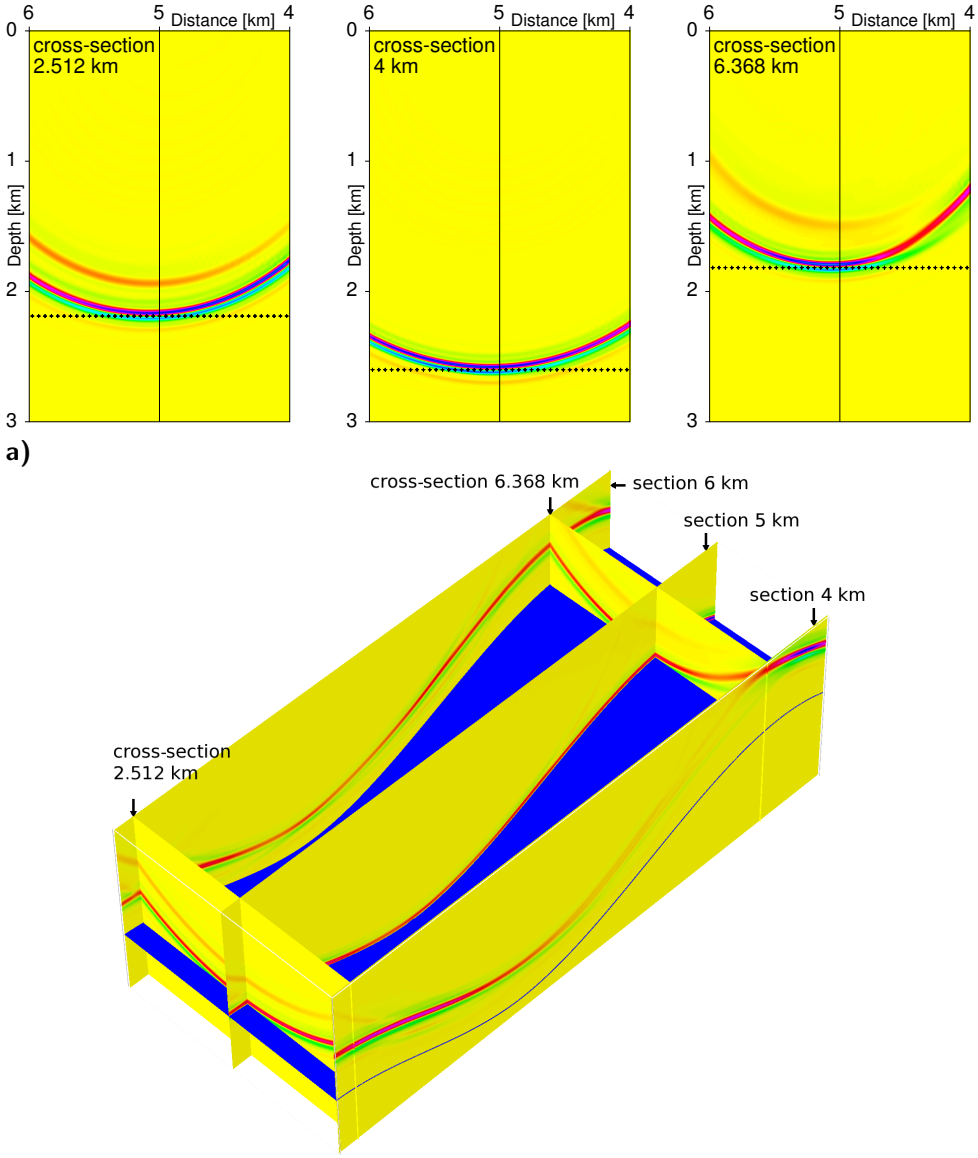

Fig. 8. The 3-D migrated volume for non-inclined curved interface corresponding to the line of sources and receivers located at $x_2 = 5$ km. The common-shot prestack depth migrated volumes corresponding to 240 sources along the profile line have been stacked. **a)** Migrated cross-sections (perpendicular to profile lines) at coordinates $x_1 = 2.512$ km, 4 km, 6.368 km. **b)** A 3-D view of the migrated volume containing 3 sections (parallel with profile lines) at $x_2 = 4$ km, 5 km, 6 km and 2 cross-sections at $x_1 = 2.512$ km, 6.368 km. The interface in the velocity model used for computation of the recorded wave field is displayed as the blue surface.

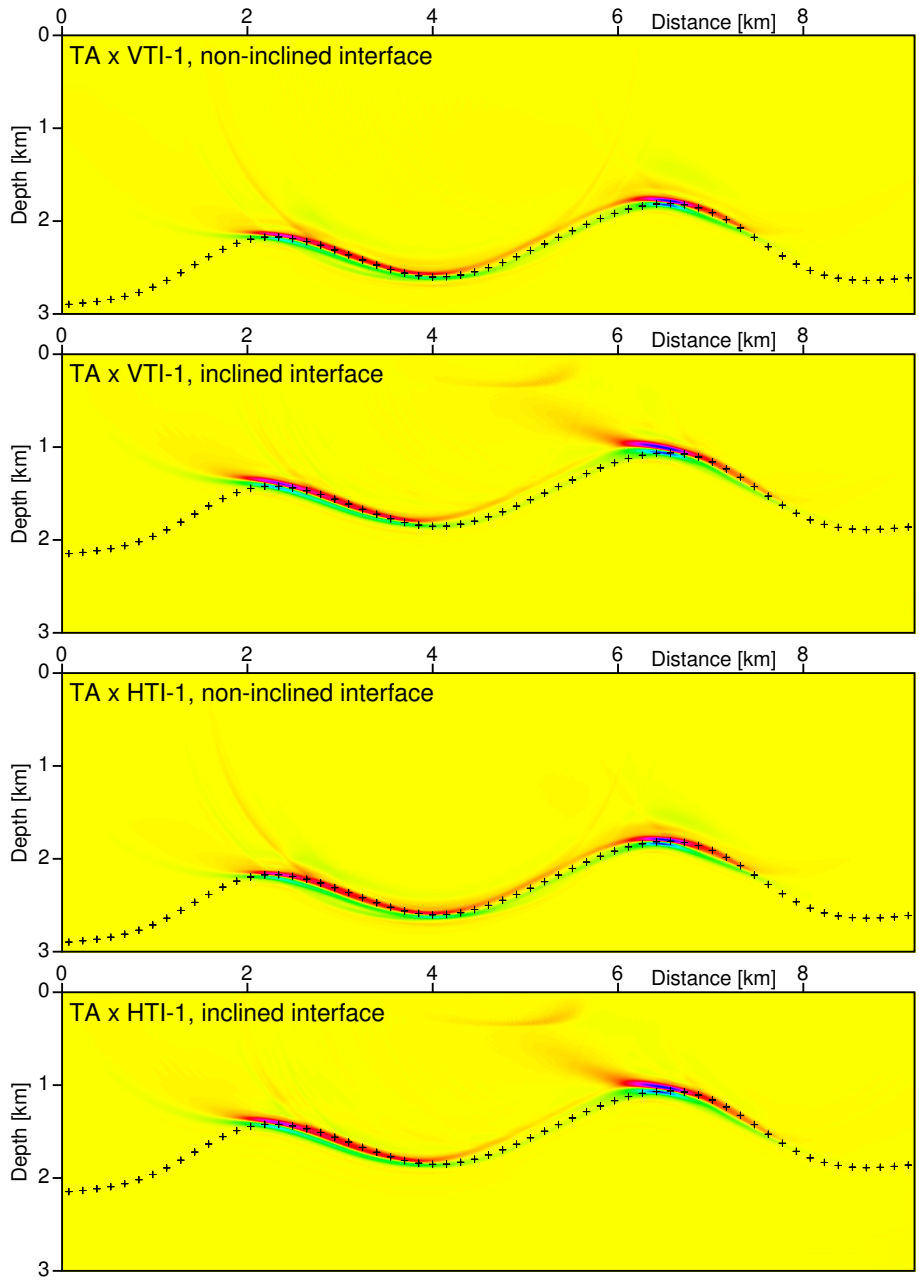

Fig. 9. Images of the centre line ($x_2 = 5$ km) generated using incorrect anisotropy models (VTI-1 and HTI-1). The correct anisotropy symmetry is triclinic (TA model). 81×240 common-shot prestack depth migrated sections, corresponding to 81 profile lines and 240 sources along each profile line, have been stacked. The crosses denote the interface in the velocity model used to compute the recorded wave field.

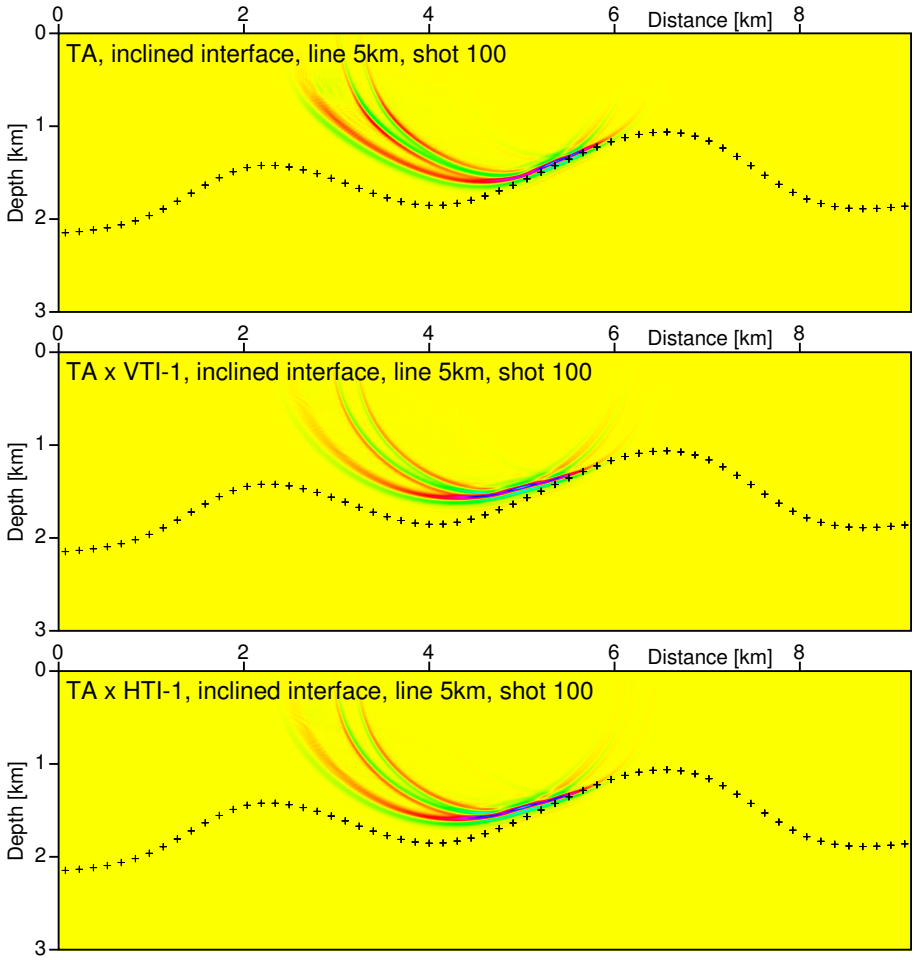

Fig. 10. Prestack depth migrated images of the single common-shot gather at line $x_2 = 5$ km corresponding to shot 100 ($x_1 = 5.475$ km), migrated using the correct triclinic anisotropy (TA) and using two incorrect anisotropies (VTI-1 and HTI-1). The crosses denote the interface in the velocity model used to compute the recorded wave field.

To explain the nearly vanishing inclined interface in the horizontal range of 4−6 km, a single common-shot image of the interface in this horizontal range is displayed in Fig. 10. Whereas the image migrated using the correct TA anisotropy is oriented correctly, the images migrated using the incorrect VTI-1 and HTI-1 anisotropies are rotated erroneously. When stacking the common-shot images, this rotation results in erasing the mentioned part of the interface due to the destructive interference.

5.2.2. Incorrect Assumption of Isotropy or Anisotropy of HTI Symmetry with the Axis Perpendicular to the Profile Lines

As in the previous experiment, the vertical P-wave velocity (matrix element A_{33}) in the isotropic (ISO) and HTI-2 models is the same as the analogous velocity (A_{33}) in the triclinic (TA) model. However, the horizontal P-wave velocity parallel with the profile lines (matrix element A_{11}) in both ISO and HTI-2 models is now equal to the vertical P-wave velocity (A_{33}) in the triclinic (TA) model. In models ISO and HTI-2 we also chose such density-reduced elastic moduli that result in approximately correct depths of the interface in the migrated image.

The migrated sections are very similar whether we migrate in the model with isotropy (ISO) or HTI-2 anisotropy (see Fig. 11). In this case the migrated interface in the horizontal range of approximately 4−6 km is displayed much better. The segments of the interface in the horizontal ranges of approximately 2−4 km and 6−8 km are defocused and mispositioned.

The poorly imaged inclined interface in the horizontal range of 2−4 km is explained in Fig. 12, showing a single common-shot image of the interface. Whereas the image migrated using the correct TA anisotropy looks well, the images migrated using the incorrect isotropy ISO and HTI-2 anisotropy are rotated and distorted. When stacking the common-shot images, this rotation and distortion lead to defocusing and mispositioning of the mentioned part of the interface.

5.2.3. VTI Velocity Model with Incorrect Vertical Velocity

In this test, we study how the VTI velocity model with incorrectly estimated vertical P-wave velocity affects the migrated image.

The vertical P-wave velocity (matrix element A_{33}) in the VTI-2 model is lower than the vertical P-wave velocity (A_{33}) in the triclinic (TA) model. The migrated interface is shifted vertically upwards (undermigrated) and is slightly distorted (see Fig. 13). The vertical shift is smaller and the distortion is greater for the model with the inclined curved interface. The migrated interface in the horizontal range of approximately 4−6 km is poorly displayed for the inclined curved interface, analogously to the migration in the VTI-1 model (see Fig. 9 in comparison with Fig. 13).

5.2.4. VTI Velocity Model with Incorrect Horizontal Velocity

In this test, we study how the VTI velocity model with correct vertical P-wave velocity but incorrectly estimated horizontal P-wave velocity affects the migrated image.

The horizontal P-wave velocity, parallel with the profile lines (matrix element A_{11}), in model VTI-3 is lower than the horizontal P-wave velocity (A_{11}) in the triclinic (TA) model (see Fig. 14). In this case we can observe the poorly displayed

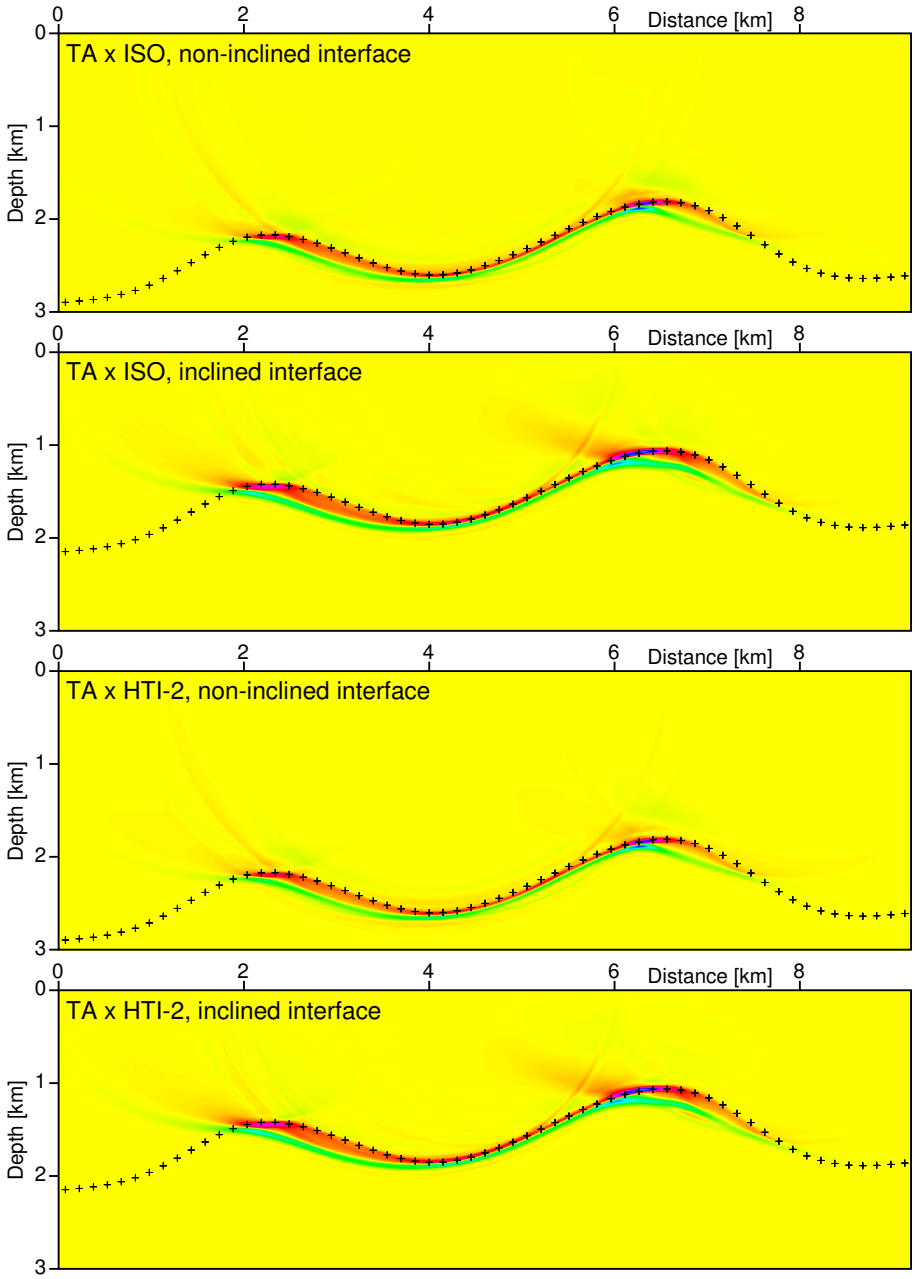

Fig. 11. Images of the centre line ($x_2 = 5$ km) generated using incorrect isotropic (ISO) and anisotropic (HTI-2) models. The correct anisotropy symmetry is triclinic (TA model). 81×240 common-shot prestack depth migrated sections, corresponding to 81 profile lines and 240 sources along each profile line, have been stacked. The crosses denote the interface in the velocity model used to compute the recorded wave field.

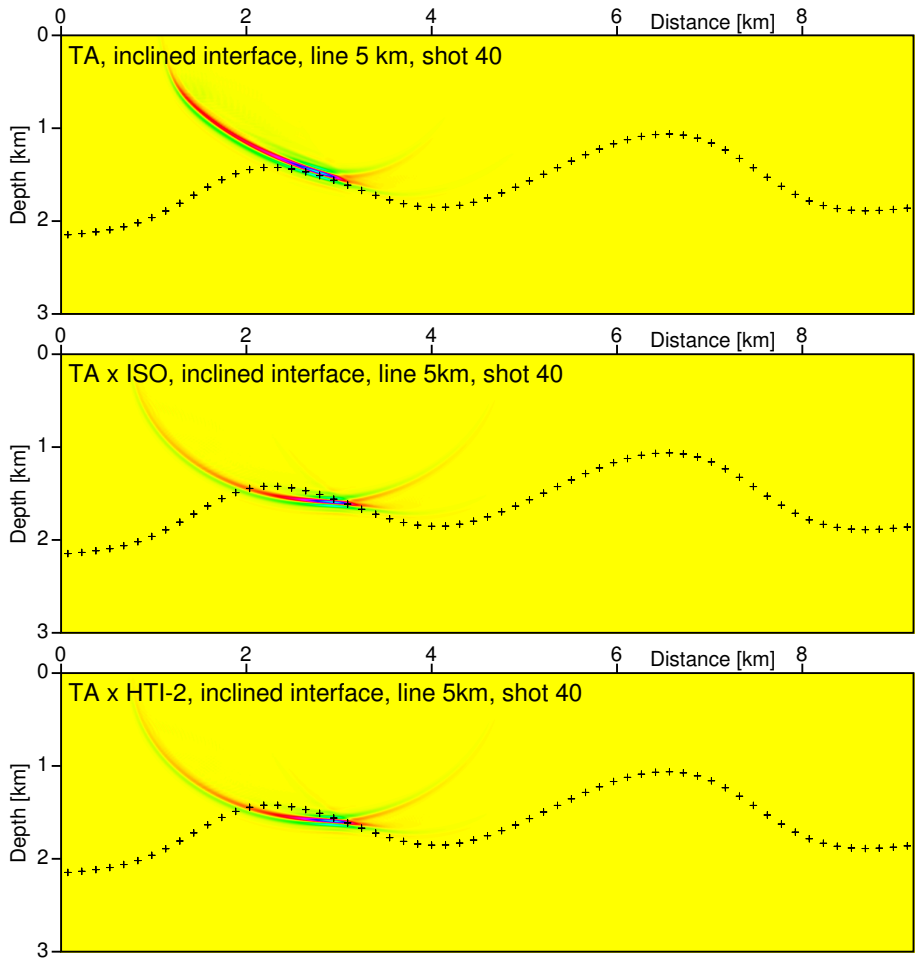

Fig. 12. Prestack depth migrated images of the single common-shot gather at line $x_2 = 5$ km corresponding to shot 40 ($x_1 = 3.975$ km), migrated using the correct triclinic anisotropy (TA) and using incorrect isotropy (ISO) and anisotropy (HTI-2). The crosses denote the interface in the velocity model used to compute the recorded wave field.

migrated interface in the horizontal range of approximately 4−6 km (as in Fig. 9). Compared with the migration in model VTI-1 (see Fig. 9 in comparison with Fig. 14), the image of the interface is slightly worse in the horizontal range of 4−6 km.

6. DISCUSSION AND CONCLUSIONS

We generated 3-D synthetic data using the ray theory in a simple velocity model of relatively strong triclinic anisotropy. We applied 3-D Kirchhoff prestack depth migration to homogeneous velocity models a) with the correct triclinic anisotropy, b) with the incorrect simpler anisotropies: isotropic medium, transversely isotropic

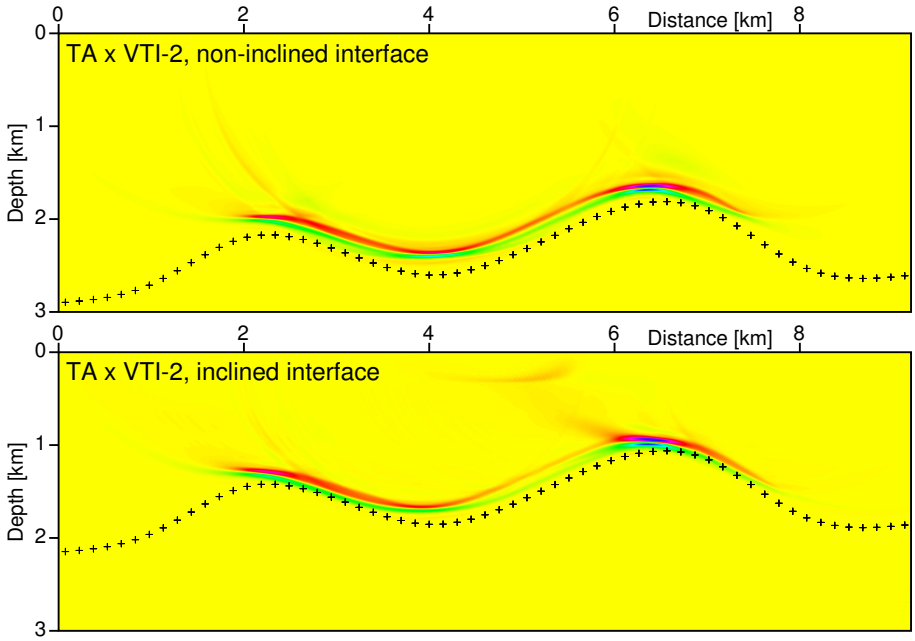

Fig. 13. Images of the centre line ($x_2 = 5$ km) generated using incorrect anisotropy model (VTI-2). The correct anisotropy symmetry is triclinic (TA model). 81×240 common-shot prestack depth migrated sections, corresponding to 81 profile lines and 240 sources along each profile line, have been stacked. The crosses denote the interface in the velocity model used to compute the recorded wave field. Compare to Fig. 9.

media with a horizontal (HTI) and vertical (VTI) symmetry axis. The study has been limited to P-waves.

In the case of correct triclinic anisotropy, the migrated interface in the final stacked image coincides nearly perfectly with the interface in the model used to compute the recorded wave field. We compared the individual contributions to the final image from eight source-receiver lines symmetrically distributed around the final image line (for the model with non-inclined curved interface). Despite the symmetrical distribution of the source-receiver lines around the final image line, we showed the apparent differences in the contributions from the corresponding symmetric pairs. The observed asymmetry in migration is caused by triclinic anisotropy that is asymmetric.

In the case of incorrect simpler anisotropies, we observed mispositioning, distortion and defocusing of the migrated interface caused by inaccurate velocity models used for migration. Different errors in the anisotropy of the velocity model influence and distort differently dipped and inclined parts of interfaces in considerably different ways. Whereas the distortion of the image due to incorrect anisotropy of the velocity model used for migration is obvious in our synthetic examples, the analogous distortion may be more difficult to identify in the images of real structures. We may also expect similar effects of the incorrect heterogeneities in the velocity model,

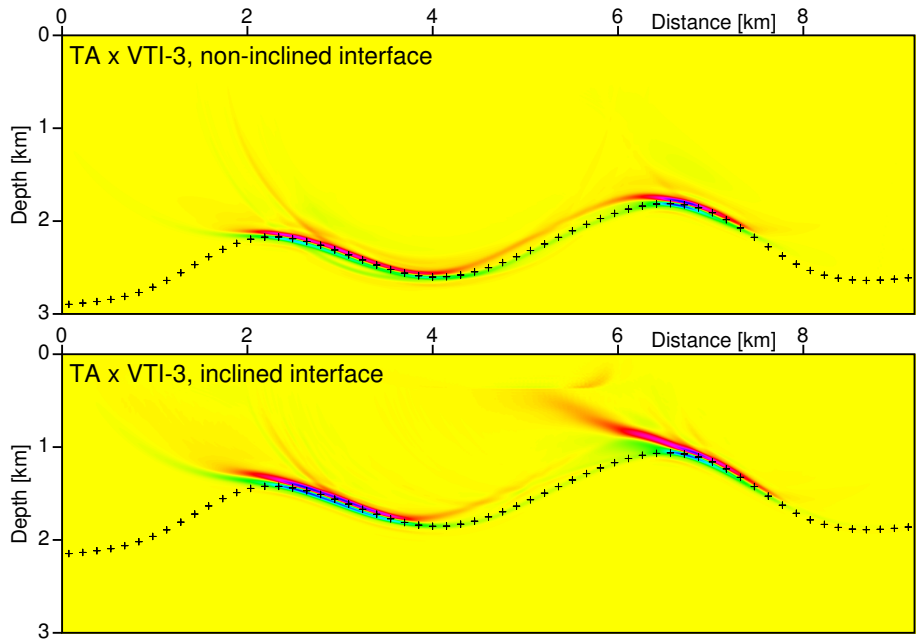

Fig. 14. Images of the centre line ($x_2 = 5$ km) generated using incorrect anisotropy model (VTI-3). The correct anisotropy symmetry is triclinic (TA model). 81×240 common-shot prestack depth migrated sections, corresponding to 81 profile lines and 240 sources along each profile line, have been stacked. The crosses denote the interface in the velocity model used to compute the recorded wave field. Compare to Fig. 9.

and synergy of the incorrect anisotropy and incorrect heterogeneities. Moreover, the influence of incorrect anisotropy and incorrect heterogeneities on the migrated image can be difficult to distinguish.

In our simple synthetic examples, the errors in images increase both with incorrect anisotropy of the velocity model and with the dip and inclination of the interface, although the heterogeneity of the velocity model is correct (the model is homogeneous).

We should take into account that the incorrect anisotropy in the velocity model for migration may result not only in the incorrect position of a single common-shot image of the interface, but also in its erroneous rotation or in its incorrect curvature. Incorrect vertical velocity (A_{33}) results in erroneous vertical positions of interfaces. Unfortunately, unless independent information is available (such as well logs), it is difficult to detect this vertical misposition in the images of a real structure. We have also demonstrated that, even for correct vertical velocity (A_{33}), the distortion of the migrated image considerably depends on the inaccuracy of the other density-reduced elastic moduli.

In the case of inaccurate anisotropy, individual common-shot images of an interface may simultaneously be positioned correctly and rotated erroneously. When stacking the common-shot images, this rotation may result in erasing some parts

of the interface due to destructive interference. In this case, improvement of the coherency between common-shot images by modifying the velocity model without correcting the anisotropy may result in sharp but mispositioned interfaces.

Acknowledgments: The author thanks Luděk Klimeš and Ivan Pšenčík for their help throughout the work on this paper. The author also thanks two anonymous reviewers and associate editor Petr Jílek for helpful comments and suggestions.

The research has been supported by the Grant Agency of the Czech Republic under contract P210/10/0736, by the Ministry of Education of the Czech Republic within research project MSM0021620860, and by the members of the consortium "Seismic Waves in Complex 3-D Structures" (see "http://sw3d.cz").

References

Alkhalifah T. and Larner K., 1994. Migration error in transversely isotropic media. *Geophysics*, **59**, 1405–1418.

Ball G., 1995. Estimation of anisotropy and anisotropic 3-D prestack depth migration, offshore Zaire. *Geophysics*, **60**, 1495–1513.

Behera L. and Tsvankin I., 2009. Migration velocity analysis for tilted transversely isotropic media. *Geophys. Prospect.*, **57**, 13–26.

Bucha V., 2010. Kirchhoff prestack depth migration in simple models of various anisotropy. In: *Seismic Waves in Complex 3-D Structures, Report 20,* Dep. Geophys., Charles Univ., Prague, 35–52, (online at http://sw3d.cz).

Bulant P., 1996. Two-point ray tracing in 3-D. *Pure Appl. Geophys.*, **148**, 421-447.

Červený V., Klimeš L. and Pšenčík I., 1988. Complete seismic-ray tracing in three-dimensional structures. In: Doornbos D.J.(Ed.), *Seismological Algorithms.* Academic Press, New York, 89–168.

Gajewski D. and Pšenčík I., 1990. Vertical seismic profile synthetics by dynamic ray tracing in laterally varying layered anisotropic structures. *J. Geophys. Res.*, **95**, 11301–11315.

Isaac J.H. and Lawton D.C., 1999. Image mispositioning due to dipping TI media: A physical seismic modeling study. *Geophysics*, **64**, 1230–1238.

Larner K. and Cohen J.K., 1993. Migration error in factorized transversely isotropic media with linear velocity variation in depth. *Geophysics*, **58**, 1454–1467.

Mensch, T. and Rasolofosaon, P., 1997. Elastic-wave velocities in anisotropic media of arbitrary symmetry-generalization of Thomsens parameters ϵ, δ and γ. *Geophys. J. Int.*, **128**, 43–64.

Tsvankin I., Gaiser J., Grechka V., Baan M. and Thomsen L., 2010. Seismic anisotropy in exploration and reservoir characterization: An overview. *Geophysics*, **75**, 75A15–75A29.

Versteeg R.J. and Grau G. (Eds.), 1991. *Proc. EAGE workshop on Practical Aspects of Seismic Data Inversion (Copenhagen, 1990)*, Eur. Assoc. Explor. Geophysicists, Zeist.

Vestrum R.W., Lawton D.C. and Schmid R., 1999. Imaging structures below dipping TI media. *Geophysics*, **64**, 1239–1246.

Vestrum R. and Lawton D., 2010. Reflection point sideslip and smear in imaging below dipping anisotropic media. *Geophys. Prospect.*, **58**, 541–548.